J|A|C|S
ARTICLES
Published on Web 03/09/2002

NMR Conformational Analysis of Antide, a Potent Antagonist of the Gonadotropin Releasing Hormone

Giuseppe Digilio,*,† Chiara Bracco,†,‡ Luca Barbero,§ Daniela Chicco,§ Maria D. Del Curto,§ Pierandrea Esposito,§ Silvio Traversa,§ and Silvio Aime‡

Contribution from the Integrated Laboratory of Advanced Methodologies, Bioindustry Park del Canavese (Bi.P.Ca.), Via Ribes 5, Colleretto Giacosa (TO), I-10010, Italy, Department of Chemistry I.F.M., University of Turin, Via P. Giuria 7, Turin, I-10125, Italy, and Istituto di Ricerca Cesare Serono−Drug Delivery Systems, Via Ribes 5, Colleretto Giacosa (TO), I-10010, Italy

Received June 25, 2001. Revised Manuscript Received November 20, 2001

Abstract: Antide is a decapeptide [(*N*-Ac-D-Nal[1]-D-Cpa[2]-D-Pal[3]-Ser[4]-Lys(Nic)[5]-D-Lys(Nic)[6]-Leu[7]-Ilys[8]-Pro[9]-D-Ala[10]-NH_2] that acts in vivo as an antagonist of GnRH (gonadotropin-releasing hormone). The conformational behavior of antide has been studied in water, TFE, DMF, and DMSO solutions by means of 2D-NMR spectroscopy and molecular dynamics calculations. Antide adopts in aqueous solution a δ-shaped backbone conformation, which is characterized by an irregular turn around residues D-Pal[3]-Ser[4] and by the close spatial proximity of the side chains belonging to D-Nal[1] and Ilys[8] (as many as 17 NOE peaks were detected between these side chains). The side-chain protons of Ilys[8] (especially the H$^\gamma$ ones) present remarkably upfield shifted resonances, because of ring current effects induced by the naphthyl moiety. The upfield shifted resonances of the Ilys[8] H$^\gamma$ hydrogen atoms are strictly characteristic of the water δ-shaped conformation and can be considered as structure markers. The observation of ring current shifted Ilys[8] H$^\gamma$ resonances under different conditions (temperature, pH, solvent) indicates a remarkable stability of the water δ-shaped conformation. Such a conformation is at least partially disrupted in solvent mixtures containing high percentages of organic solvents. TFE can induce a well-defined conformation, which is characterized by an S-shaped backbone conformation. In DMF and DMSO solution, the molecule is basically endowed with a random coil conformation and high fluxionality. Antide fulfills the conformational requirements that are known to play a crucial role in receptor recognition, namely (i) the presence of a turn in the backbone and (ii) the all-trans nature of peptide bonds. In addition, the structural rigidity of antide likely adds a further contribution to the receptor binding affinity.

Introduction

Antide is a unnatural decapeptide (*N*-Ac-D-Nal[1]-D-Cpa[2]-D-Pal[3]-Ser[4]-Lys(Nic)[5]-D-Lys(Nic)[6]-Leu[7]-Ilys[8]-Pro[9]-D-Ala[10]-NH_2) that acts in vivo as a highly potent and reversible antagonist of the gonadotropin releasing hormone (GnRH), thereby inhibiting the release of pituitary gonadotropins. Due to its in vivo potency and to the fact that antide shows minimal toxic side effects (e.g., minimal histamine release activity),[1] it has become very promising for the treatment of fertility disorders and was subjected to clinical investigations.[2] Although in principle antide may be also useful in the treatment of hormone-dependent tumors, this application is somewhat hampered by its limited solubility in physiological media. The amino acid sequence of antide has been thoroughly optimized by means of a structure−activity relationship approach, where the role of each amino acid in the primary structure has been analyzed in terms of antiovulatory potency,[3] receptor binding affinity, and minimization of the undesired toxic effects due to histamine release activity.[3,4]

Despite the considerable mass of data concerning the biological activity and in vivo testing, only little effort was paid to the investigation of the structural and conformational features underlying at the molecular level the potency of antide as an antagonist of GnRH. The lack of molecular insights into the mechanisms that lead to the interaction with its receptor is mainly due to the complexity of the receptor, an integral membrane protein that belongs to the G protein-coupled receptor (GPCR) superfamily.[5] However, several structural studies on a number of GnRH analogues pointed out that conformational

* To whom correspondence should be addressed. Phone +39 0125 538346. Fax: +39 0125 538350. E-mail: chemlima@bioindustrypark.it.
† Bioindustry Park del Canavese.
‡ University of Turin.
§ Istituto di Ricerca Cesare Serono−Drug Delivery Systems.

(1) Ljungqvist, A.; Feng, D. M.; Tang, P. F. L.; Kubota, M.; Okamoto, T.; Zhang, Y.; Bowers, C.; Hook, W. A.; Folkers, K. *Biochem. Biophys. Res. Commun.* **1987**, *148*, 849−856.
(2) Bagatelle, C. J.; Conn, P. M.; Bremner, W. J. *Fertility Sterility* **1993**, *60*, 680−685.
(3) Flouret, G.; Arnold, Z. S.; Majewski, T.; Petousis, N. H.; Mahan, K.; Farooqui, F.; Blum, K. A.; Konopinska, D.; Natarajan, S.; Crich, D. *J. Pept. Sci.* **1995**, *1*, 89−105.
(4) Bajusz, S.; Csernus, V. J.; Janaky, T.; Bokser, L.; Fekete, M.; Schally, A. V. *Int. J. Pept. Protein Res.* **1988**, *32*, 425−435.
(5) Flanagan, C. A.; Millar, R. P.; Illing, N. *Rev. Reproduction* **1997**, *2*, 113−120.

requirements have an important contribution to receptor binding and activation (reviewed in ref 6), and they should be accounted for in drug design and optimization. Among such requirements, the all-trans nature of peptide bonds and the presence of a β-type turn appear to be crucial to yield a biologically active conformation both for agonists and antagonists. The central role of the chain reversal brought about by this turn was also indicated by the fact that the native GnRH itself, although highly fluxional, can adopt a type II β-turn conformation around residues 5−8.[7−10] The presence of a turn in the peptide backbone is often ensured by the presence of an amino acid in the D-configuration at position 6, and analogues having a D-amino acid in that position usually show high binding affinities.[5,6,11,12] However, this substitution does not necessarily provide by itself a suitable conformational rigidity. To stabilize such a conformation, a number of covalently constrained dicyclic analogues of GnRH were synthesized and found to be endowed with high potency.[13,14] Since the backbone conformation and the location of the β-turns along the backbone was different in dicyclic analogues endowed with very similar sequences and constraints, it was concluded that (i) more than one conformation may be biologically relevant or (ii) some conformational change may still take place upon receptor binding.

It must be emphasized that, beside the backbone conformation, also the spatial orientation of the side chains must have a role in the receptor binding activity. In the case of GnRH agonists, it was suggested that the binding affinity to the receptor is increased if the spatial arrangement of the tripeptide N-terminal fragment is such to provide a clustering of three aromatic rings.[15] However, since the sites of interaction of GnRH and its antagonists with the receptor may only partially overlap in space,[5] care must be exercised when attempting to extend the results obtained for GnRH agonists to the antagonists.

To the best of our knowledge, no detailed conformational analysis of antide has been carried out. In this paper we worked out the three-dimensional structure of antide in water and organic solvents by means of 2D-NMR spectroscopy. Such a structural characterization is believed to provide a basis for the understanding of the conformational contribution to the potency of antide as a GnRH antagonist.

Methods

NMR Spectroscopy. Antide (acetate salt) was purchased from Bachem AG (Bubendorf, CH). The concentration of antide for NMR investigations was typically 0.5 mM for experiments carried out in water. If required, the pH was adjusted by means of 0.1 M HCl or 0.1 M NaOH. Antide concentration in organic solvent solutions (TFE-d_2-OH, DMSO-d_6, and DMF-d_7) ranged from 0.7 to 4.2 mM. The complete list of sample conditions used to obtain 2D-NOESY data for the structural calculations is given in Table 4. NMR experiments were carried out on a Bruker Avance 600 MHz spectrometer operating at 14 T (corresponding to a resonance frequency of 600 MHz for the ^{1}H nucleus) equipped with a triple axis-PFG probe optimized for ^{1}H detection. Water suppression was achieved by means of presaturation of the solvent line during the recycle delay in the case of D_2O solutions or by the WATERGATE technique in the case of H_2O/D_2O (typically 90:10) mixtures. Chemical shifts were referenced to an external solution (coaxial insert) containing 0.03% TMS in deuterated chloroform ($CDCl_3$). 2D-TOCSY experiments were carried out with the MLEV17 mixing scheme at a spin locking field strength of 9 kHz, and the STATES-TPPI phase cycling was used to obtain complex data points in the t_1 dimension. Typically, the following instrumental settings were used for TOCSY experiments: spectral width 6900 Hz, 512 and 2048 complex data points in the t_1 and t_2 dimensions respectively, 32−64 scans per t_1 increment, relaxation delay 3 s, mixing time 100 ms. The data were apodized with a square cosine window function and zero-filled to a matrix of size 1024 × 1024 prior to FT and baseline correction.

2D-NOESY experiments were carried out by the standard pulse sequence with the STATES-TPPI phase cycling scheme with mixing times ranging from 120 up to 400 ms. Typical instrumental settings included spectral width 6900 Hz in both f_1 and f_2, 2048 × 512 data points in t_2 and t_1 respectively, 32−64 scans per t_1 increment, recycle delay 3 s. The data were apodized along both t_1 and t_2 dimensions with a square cosine window function and zero-filled to a symmetrical matrix of size 1024 × 1024 data points prior to Fourier transformation and baseline correction.

2D-DQF−COSY (double quantum filtered correlation spectroscopy) experiments were obtained in the phase sensitive mode by means the TPPI method with the standard double quantum filtered pulse sequence coupled with a combination of PFG at the magic angle and selective water excitation to achieve optimal water suppression.[16] Typical instrumental settings included spectral width 6600 Hz in f_1 and f_2, 4096 × 512 data points in t_2 and t_1, recycle delay 3 s, 104 scans per t_1 increment. The data were apodized with a square cosine window function and zero-filled to a matrix of size 2048 × 1024 prior to FT and baseline correction.

Molecular Dynamics and Energy Minimization. The assignment of NMR signals and integration of NOE peaks were done by means of the XEASY[17] software package. The assignment of ^{1}H NMR resonances was carried out by the sequence-specific method,[18] i.e. by iterative comparison of TOCSY, NOESY, and DQF−COSY spectra. A number of ambiguities in the assignment due to severe signal overlap could be resolved by comparing experiments carried out at different temperatures or pH. The structure optimization based on NMR constraints was carried out by the programs DYANA[19] (energy minimization by torsion angle dynamics and simulated annealing, TAD) and MOLMOL[20] (molecular graphics). Peak volumes were obtained from NOESY spectra acquired with mixing times of 300−350 ms (see also Table 4). At these mixing times, no significant spin diffusion effects were found. The peak volumes were converted into pairwise interproton upper limit distances as described in ref 21. To account for the effect of local motions on

(6) Sealfon, S. C.; Weinstein, H.; Millar, R. P. *Endocr. Rew.* **1997**, *18*, 180−205.
(7) Maliekal, J. C.; Jackson, G. E.; Flanagan, C. A.; Millar, R. P. *S. Afr. J. Chem.* **1997**, *50(4)*, 217−219.
(8) Guarnieri, F.; Weinstein, H. *J. Am. Chem. Soc.* **1996**, *118*, 5580−5589.
(9) Mezei, M.; Guarnieri, F. *J. Biomol. Struct. Dyn.* **1998**, *16(3)*, 723−732
(10) (a) Nikiforovich, G. V.; Marshall, G. R. *Int. J. Pept. Protein Res.* **1993**, 42, 171−180. (b) Nikiforovich, G. V.; Marshall, G. R. *Int. J. Pept. Protein Res.* **1993**, *42*, 181−193.
(11) Chandrasekaran, R.; Lakshminarayanan, A. V.; Pandya, U. V.; Ramachandran, G. N. *Biochim. Biophys. Acta* **1973**, *303*, 14−27.
(12) Monahan, M. W.; Amoss, M. S.; Anderson, H. A.; Vale W. *Biochemistry* **1973**, *12*, 4616−4620.
(13) Bienstock, R. J.; Rizo, J.; Koerber, S. C.; Rivier, J. E.; Hagler, A. T.; Gierasch, L. M. *J. Med. Chem.* **1993**, *36*, 3265−3273.
(14) (a) Rizo, J.; Sutton, R. B.; Breslau, J.; Koerber, S. C.; Porter, J.; Hagler, A. T.; Rivier, J. E.; Gierasch, L. M. *J. Am. Chem. Soc.* **1996**, *118*, 970−976. (b) Rizo, J.; Koerber, S. C.; Bienstock R. J.; Rivier J.; Gierasch, L. M.; Hagler, A. T. *J. Am. Chem. Soc.* **1992**, *114*, 2860−2871.
(15) Matsoukas, J. M.; Keramida, M.; Panagiotopoulos, D.; Mavromoustakos, T.; Maia H. L. S.; Bigam, G.; Pati, D.; Habibi, H. R.; Moore, G. J. *Eur. J. Med. Chem.* **1997**, *32*, 927−940.
(16) John, B. K.; Plant, D.; Webb, P.; Hurd, R. E. *J.Magn.Res.* **1992**, *98*, 200−206.
(17) Bartels, C.; Xia, T.-H.; Billeter, M.; Güntert, P.; Wüthrich, K. *J. Biomolecular NMR* **1995**, *6*, 1−10.
(18) Wüthrich K. *NMR of proteins and nucleic acids;* John Wiley and Sons: New York, 1986.
(19) Güntert, P.; Mumenthaler, C.; Wüthrich, K. *J. Mol. Biol.* **1997**, *273*, 283−298.
(20) Koradi, R.; Billeter, M.; Wüthrich, K. *J. Mol. Graphics* **1996**, *14*, 51−55.
(21) (a) Güntert, P.; Braun, W.; Wüthrich, K. *J. Mol. Biol.* **1991**, *217*, 517−530. (b) Güntert, P. *Quart. Rev. Biophys.* **1998**, *31(2)*, 145−237.

Table 1. ^{1}H NMR Chemical Shifts of Antide in Different Solvents[e]

residue	^{1}H atom	δ, ppm			
		water[a]	TFE[b]	DMF[c]	DMSO[d]
$-CH_3CO$	$-CH_3$	1.81	1.90	1.81	1.68
D-Nal[1]	HN	8.51	7.46	8.39	8.21
	H^{α}	5.04	4.66	4.77	4.59
	$H^{\beta 1}/H^{\beta 2}$	3.14, 2.91	3.14, 3.04	3.23, 2.98	3.02, 2.77
	$H^{\delta 2}$	7.20	7.24	7.74	7.32
	$H^{\epsilon 2}$	7.73	7.74	7.83	7.74
	$H^{\delta 1}$	7.57	7.58	7.43	7.63
	$H^{\eta 2}/H^{\vartheta}/H^{\eta 1}/H^{\zeta 1}$	7.81 ($H^{\eta 2}$), 7.39, 7.43, 7.62 ($H^{\zeta 1}$)	7.77 ($H^{\eta 2}$), 7.41, 7.43, 7.73 ($H^{\zeta 1}$)	7.50 ($H^{\eta 2}$), 7.49, 7.90, 7.82	7.82 ($H^{\eta 2}$), 7.43, 7.44, 7.76 ($H^{\zeta 1}$)
D-Cpa[2]	HN	8.88	7.65	8.58	8.21
	H^{α}	4.70	4.35	4.71	4.50
	$H^{\beta 1}/H^{\beta 2}$	3.23, 2.61	3.04, 2.79	3.21, 2.97	3.00, 2.74
	$H^{\delta 2}$	7.05	6.88	7.30	7.18
	$H^{\epsilon 2}$	7.10	7.09	7.55	7.21
D-Pal[3]	HN	8.74	7.47	8.69	8.39
	H^{α}	4.22	4.29	4.76	4.61
	$H^{\beta 1}/H^{\beta 2}$	3.22, 2.98	3.17, 2.92	3.23, 3.10	3.01, 2.87
	$H^{\delta 1}$	8.36	8.24	8.58	8.42
	H^{ζ}	8.45	8.35	8.45	8.37
	$H^{\epsilon 2}$	7.44	7.35	7.33	7.28
	$H^{\delta 2}$	7.73	7.61	7.79	7.66
Ser[4]	HN	8.33	7.60	8.66	8.32
	H^{α}	4.09	4.34	4.50	4.33
	$H^{\beta 1}/H^{\beta 2}$	3.64, 3.10	3.99, 3.65	3.87, 3.63	3.56, 3.40
Lys(Nic)[5]	HN	8.00	7.81	8.55	8.13
	H^{α}	4.12	4.26	4.31	4.17
	$H^{\beta 1}/H^{\beta 2}$	1.73	1.94, 1.84	1.94, 1.83	1.69, 1.60
	$H^{\gamma 1}/H^{\gamma 2}$	1.32, 1.15	1.50, 1.41	1.42	1.25
	$H^{\delta 1}/H^{\delta 2}$	0.97	1.54	1.55	1.39
	$H^{\epsilon 1}/H^{\epsilon 2}$	2.80, 2.68	3.28	3.33	3.14
	HN^{ζ}	8.00	7.62	8.80	8.63
	$H^{\iota 1}$	8.46	8.77	9.15	8.91
	H^{λ}	8.62	8.55	8.74	8.65
	$H^{\kappa 2}$	7.47	7.44	7.54	7.46
	$H^{\iota 2}$	7.83	8.06	8.32	8.10
D-Lys(Nic)[6]	HN	7.45	7.58	8.13	7.81
	H^{α}	4.52	4.28	4.34	4.26
	$H^{\beta 1}/H^{\beta 2}$	1.83, 1.76	1.90, 1.82	1.86, 1.79	1.63, 1.52
	$H^{\gamma 1}/H^{\gamma 2}$	1.48, 1.39	1.51, 1.42	1.52, 1.42	1.25
	$H^{\delta 1}/H^{\delta 2}$	1.70	1.65	1.63	1.48
	$H^{\epsilon 1}/H^{\epsilon 2}$	3.46, 3.41	3.42, 3.36	3.41, 3.36	3.21
	HN^{ζ}	8.57	7.78	8.80	8.69
	$H^{\iota 1}$	8.66	8.82	9.14	8.95
	H^{λ}	8.56	8.56	8.74	8.65
	$H^{\kappa 2}$	7.42	7.46	7.53	7.48
	$H^{\iota 2}$	7.98	8.13	8.29	8.14
Leu[7]	HN	8.78	7.55	8.21	8.13
	H^{α}	4.59	4.42	4.52	4.33
	$H^{\beta 1}/H^{\beta 2}$	1.61, 1.58	1.68	1.68, 1.65	1.41, 1.34
	H^{γ}	1.48	1.57	1.57	1.49
	$H^{\delta 1}{}_3/H^{\delta 2}{}_3$	0.89, 0.84	0.91, 0.85	0.88, 0.82	0.80, 0.75
Ilys[8]	HN	7.71	7.46	8.02	8.06
	H^{α}	3.36	4.49	4.49	4.20
	$H^{\beta 1}/H^{\beta 2}$	1.02, 0.80	1.63, 1.60	1.72, 1.51	1.53, 1.32
	$H^{\gamma 1}/H^{\gamma 2}$	−0.04, −0.09	1.21	1.38, 1.34	1.22
	$H^{\delta 1}/H^{\delta 2}$	1.15, 0.97	1.40, 1.35	1.50	1.42
	$H^{\epsilon 1}/H^{\epsilon 2}$	2.63, 2.60	2.95	2.68	2.67
	$HN^{\zeta}{}_2$	7.92			
	H^{η}	3.25	3.30	2.96	3.07
	$H^{\vartheta 1}{}_3/H^{\vartheta 2}{}_3$	1.26, 1.22	1.31	1.11	1.10
Pro[9]	H^{α}	4.26	4.34	4.39	4.21
	$H^{\beta 1}/H^{\beta 2}$	2.23, 1.81	2.25, 1.92	2.11, 1.90	2.02, 1.74
	$H^{\gamma 1}/H^{\gamma 2}$	1.97, 2.03	2.10	2.06, 1.89	1.94, 1.78
	$H^{\delta 1}/H^{\delta 2}$	3.77, 3.21	3.79, 3.49	3.86, 3.61	3.74, 3.44
D-Ala[10]	HN	8.75	7.91	8.42	8.35
	H^{α}	4.15	4.20	4.26	4.07
	$H^{\beta}{}_3$	1.34	1.40	1.31	1.19
$-NH_2$	$-NH_2$	7.10	7.49	7.48	7.27
		7.46	6.26	7.22	7.08

[a] Antide 0.5 mM, H_2O/D_2O 90%, pH = 5.1, T = 280 K. Chemical shifts referenced to external TMS in chloroform-*d* solution. [b] Antide 3.5 mM, neat TFE-d_2-OH, T = 285 K. Chemical shifts referenced to TMS using the signal of TFE at 3.88 ppm as a secondary standard. [c] Antide 4.2 mM, neat DMF-d_7, T = 280 K. Chemical shifts referenced to TMS using the high field methyl resonance of DMF at 2.75 ppm as a secondary standard. [d] Antide 0.7 mM, DMSO-d_6/H_2O 90%, T = 290 K. Chemical shifts referenced to internal TMS. [e] The assignment of diastereotopic atom pairs is not stereospecific

Table 2. Coupling Constants $^3J_{NH-H\alpha}$ in Antide[a]

residue	$^3J_{NH-H\alpha}$ (Hz)	residue	$^3J_{NH-H\alpha}$ (Hz)
D-Nal[1]	8.7	D-Lys(Nic)[6]	7.5
D-Cpa[2]	8.3	Leu[7]	7.5
Ser[4]	7.5	Ilys[8]	4.7
Lys(Nic)[5]	6.3		

[a] Measured in H_2O/D_2O 90%, pH = 5.1.

Table 3. Temperature Coefficients of Antide Amide Protons (0.5 mM, H_2O/D_2O 90%, pH = 5.1) and Solvent Accessible Surfaces Calculated from the Molecular Models (families $\delta 1$ and $\delta 2$)[a]

amide proton	$\Delta\delta/\Delta T$ (ppb/K)	solvent accessible surface Å^2 ± sd	
		family $\delta 1$[b]	family $\delta 2$[c]
D-Nal[1] NH	−11.8	5.3 ± 1.2	4.6 ± 1.4
D-Cpa[2] NH	−14.0	0.0 ± 0.0	0.0 ± 0.0
D-Pal[3] NH	−14.3	0.3 ± 0.2	0.0 ± 0.0
Ser[4] NH	−6.1	1.2 ± 0.6	0.0 ± 0.0
Lys(Nic)[5] NH	−2.1	0.0 ± 0.0	0.0 ± 0.0
D-Lys(Nic)[6] NH	+5.0	0.0 ± 0.0	0.0 ± 0.0
Leu[7] NH	−15.2	3.1 ± 1.2	4.1 ± 1.6
Ilys[8] NH	+3.0	0.7 ± 0.7	0.0 ± 0.0
D-Ala[10] NH	−11.3	4.2 ± 5.2	1.6 ± 2.9
Lys(Nic)[5] NH$^\zeta$	−0.3	4.0 ± 2.8	4.3 ± 2.7
D-Lys(Nic)[6] NH$^\zeta$	−6.2	6.1 ± 2.9	6.0 ± 2.0

[a] A probe radius of 1.4 Å was used in solvent accessible surface calculations. [b] Mean values ± sd calculated over 13 structures. [c] Mean values ± sd calculated over 17 structures.

Table 4. Summary of the NMR Derived Constraints Used for Torsion Angle Dynamics (TAD) with Simulated Annealing Calculations and Results from Structure Optimization

	water[a]	TFE[b]	DMF[c]	DMSO[d]
Interproton Upper Distance Bounds from NOEs				
total number	180	193	141	109
intraresidue	63	112	66	59
$i, i+1$	63	58	62	49
$i, i+2$	2	7	11	1
$i, i+3$	1	6	2	0
$i, i+4$	18	6	0	0
$i, i+5$ or more	33	4	0	0
Torsion Angle Restraints				
number of $^3J_{NH-H\alpha}$	7	3	8	0
Structure Calculation				
accepted conformers[e]	30	30	30	30
target function (Å^2)[f]	0.04 ± 0.01	0.11 ± 0.02	0.13 ± 0.02	0.07 ± 0.004
violations of upper limit bounds[g]				
violation > 0.2 Å	0	0	0	0
violation > 0.1 Å	1	3	5	1
violation of van der Waals lower bounds[g]				
violation > 0.1 Å	0	0	0	0

[a] Antide 0.5 mM, H_2O/D_2O 90%, pH = 5.1, T = 280 K, NOESY mixing time 350 ms; antide 0.5 mM, D_2O, pH = 5.3, T = 280 K, NOESY mixing time 350 ms. The numer of upper limit distances reported in the table is the sum of the ones obtained from H_2O spectra and D_2O spectra. [b] Antide 3.5 mM, neat TFE-d_2-OH, T = 285 K, NOESY mixing time 300 ms. [c] Antide 4.2 mM, neat DMF-d_7, T = 280 K, NOESY mixing time 350 ms. [d] Antide 0.7 mM, DMSO-d_6/H_2O 90%, T = 290 K, NOESY mixing time 300 ms. [e] Selected out of 1000 minimized conformers. [f] Averaged over all accepted conformers. [g] Violations consistently found in at least one-third of the accepted structures.

the intensity of the NOE signals, the peak volume-to-internuclear upper limit bound conversion was executed by classifying the NOEs into three different calibration classes and applying to each of them a different calibration function: (i) NOE peaks between backbone protons (amide protons, H^α and H^β) were converted with the function $V = A/d^6$; (ii) NOE peaks involving side-chain protons (except H^β and methyl groups) were calibrated with the function $V = B/d^4$; and (iii) NOE peaks involving methyl groups were calibrated with the function $V = C/d^4$. To obtain an initial guess of the parameters A, B, and C, the parameter A was set such that the average upper limit distance between the backbone protons became 3.6 Å. The parameters B and C were calculated accordingly such that the calibration curves intersected at the minimally allowed upper distance limit (set to 2.4 Å). Then, parameters A, B, and C were optimized by trial and error in preliminary TAD calculations until a self-consistent set of restraints was achieved. Upper distance limits involving diastereotopic atom pairs without stereospecific assignment were increased in order to allow for both assignments as described in ref 21. Dihedral ϕ-angle constraints were derived from $^3J_{NH-H\alpha}$ by using the Karplus equation, $^3J_{NH-H\alpha} = A + B\cos\vartheta + C\cos^2\vartheta$, where the values $A = 1.9$, $B = -1.4$, and $C = 6.4$ were used.

All the structure optimization calculations were carried out on a Silicon Graphics Octane workstation. The conformation of the molecule was optimized by means of molecular dynamics in the torsion angle space (TAD) coupled with simulated annealing. As many as 1000 conformers with all-trans peptide bonds geometry and random values of all ϕ, ψ, and χ dihedral angles were generated. Bond lengths and bond angles were kept fixed at their optimal values according to the ECEPP/2 [22] standard geometry. The initial random conformers were independently minimized by performing 100 conjugate gradient minimization steps including only distance constraints between atoms up to three residues far apart in the sequence. Hydrogen atoms were not considered explicitly to check for steric overlap. One hundred more conjugate gradient minimization steps were done with the complete set of restraints. Then each random conformer underwent up to 1000 TAD steps at an equilibration reference temperature of 9600 K with an initial time-step of 2 fs, followed by 4000 TAD steps with slow cooling close to zero temperature. The hydrogen atoms were then explicitly included in the check for steric overlap and 100 conjugate gradient minimization steps were performed, followed by 200 TAD steps at zero reference temperature. In the end, 1000 final conjugate gradient minimization steps were taken. Throughout these calculations, the contribution to the target function due to the violation of upper limit distance constraints was measured according to a square potential function. The optimized conformers were ranked according to increasing residual target function values (which describes the consistency of the optimized conformers with the experimental constrains) and accepted if their residual target function values were below the cutoff value of 0.2 Å^2 and if they did not present any consistent steric or geometric violation. Typically, as many as 30 conformers endowed with the lowest final target function values were chosen to be representative of the peptide structure and refined further by restrained molecular dynamics simulations followed by energy minimizations. Such calculations were performed with the MACROMODEL 6.5 [23] software package (Columbia University, NY). The potential energy calculations were done according to the AMBER force field.[24] All hydrogens were considered explicitly, and the Ilys[8] secondary amino group was considered as positively charged. MD simulations were done according to the algorithms described in ref 25. Molecular dynamics were performed at a constant bath temperature of 300 K with a time step of 1.5 fs for a total simulation length of typically 10 ps. Energetic restraints to the interatomic distances obtained from NOE data were supplied by a flat-bottom potential well. This potential is null below the upper limit distance and increases quadratically when the interatomic distance exceeds the upper distance limit with a force constant of 100 kJ mol^{-1}

(22) Nèmethy, G.; Pottle, M. S.; Scheraga, H. A. *J. Phys. Chem.* **1983**, *87*, 1883−1887.
(23) Mohamadi, F.; Richards, N. G. J.; Guida, W. C.; Liskamp, R.; Lipton, M.; Caufield, C.; Chang, G.; Hendrickson, T.; Still, W. C. *J. Comput. Chem.* **1990**, *11*, 440−467.
(24) (a) Weiner, S. J.; Kollman, P. A.; Case, D. A.; Singh, U. C.; Chio, C.; Alagona, G.; Profeta, S.; Weiner, P. *J. Am. Chem. Soc.* **1984**, *106*, 765−784. (b) McDonald, D. Q.; Still, W. C. *Tetrahedron Lett.* **1992**, *33*, 7743−7746.
(25) (a) Ryckaert, J. P.; Ciccotti, G.; Berendsen, H. J. C. *J. Comput. Phys.* **1977,** 23, 327−341. (b) van Gunsteren, W. F.; Berendsen, H. J. C. *Mol. Simulation* **1998**, 1,173−185.

Å^{-2}. No torsional restraint was used in molecular dynamics simulations. Energy minimizations were carried out by means of the Polak−Ribiere conjugate gradient minimization mode through 500 iteration molecular mechanics cycles. The value of the derivative convergence criterion used was 0.5 kJ mol^{-1} Å^{-1}. Energy minimizations were performed including water solvation as well as in vacuo. The treatment of the solvent was done according to the generalized Born/surface area (GB/SA) continuum solvation model.[26] The calculation of the solvent accessible surface at individual amide atoms was carried out by the standard MACROMODEL tools, using a probe radius of 1.4 Å to simulate a water molecule. The similarity between three-dimensional structures was quantified in terms of root-mean-square deviation (rmsd) for a given set of corresponding atoms (e.g., backbone and/or heavy atoms) after optimal rigid body superpositioning of the structures. The clustering of the structures within a given ensemble into structurally related families was done by means of cluster analysis as implemented in the XCLUSTER software package (Columbia University, NY).[27] Atomic rms displacements between pairs of structures after rigid body superpositioning were used to generate the distance matrix to be searched for clusters.

Results

Aqueous Solution. (A) ^{1}H NMR Resonance Assignment. At a level of 9.4 mM, antide forms a very viscous solution. The ^{1}H NMR spectrum recorded at high antide concentration (D_2O, 300 K) shows broad and poorly resolved signals, also at temperatures as high as 333 K. At lower concentrations the line width decreases, and the concentration of 0.5 mM appears to be a good compromise between an acceptable ^{1}H NMR line width, a low degree of aggregation phenomena, and instrumental time requirement for 2D-NMR data acquisition. Due to the high viscosity of antide aqueous solutions, the condition of slow motion ($\omega^2\tau_c^2 \gg 1$, where ω is the Larmor frequency for the ^{1}H nucleus and τ_c is the correlation time for the molecular motion) is satisfied, thereby ensuring a high sensitivity of NOESY experiments. At the temperature of 280 K, the rate of exchange of backbone and side-chain amide protons is such to yield sharp signals, from which most of the $^3J_{NH-H\alpha}$ coupling constants values can be directly read (Table 2).

The ^{1}H NMR spectra of antide show one signal for each proton present in the molecule, also when they are acquired under different conditions in terms of pH, temperature, and solvent. Thus, no evidence can be found about the presence of slowly interchanging conformers (on the NMR time scale) or about the presence of asymmetric dimeric/oligomeric species. The ^{1}H NMR resonance assignment procedure led to the following observations:

(1) H^α,H^β, H^γ, H^δ, H^ϵ protons belonging to the aliphatic side-chains protons of the three lysine-like residues [Lys(Nic)^5, D-Lys(Nic)^6, and Ilys^8] show a remarkable spread in their chemical shift values (Figure 2, Table 1). This indicates that the average chemical environment of each of these residues is different.

(2) The protons belonging to the side chain of residue Ilys^8 (mainly H^γ and H^δ) were found to have chemical shift values much more upfield than expected for lysine-like protons. Moreover, such signals show a larger line width (ca 20 Hz) than the other aliphatic signals (3−4 Hz). These effects may be due to the proximity of an aromatic ring (ring current shift effect) and to the presence of dynamical processes. The chemical shift of H^α, H^γ, and H^δ belonging to Ilys^8 are very sensitive to changes in solvent and temperature (Figures 2−4). The H^γ and H^δ side chain protons of Lys(Nic)^5 also present upfield shifted resonances, even though this upfield shift is much less evident than in the case of Ilys^8. As found for the Ilys^8 side-chain protons, the chemical shifts of H^γ and H^δ of Lys(Nic)^5 are very sensitive to changes in temperature and solvent.

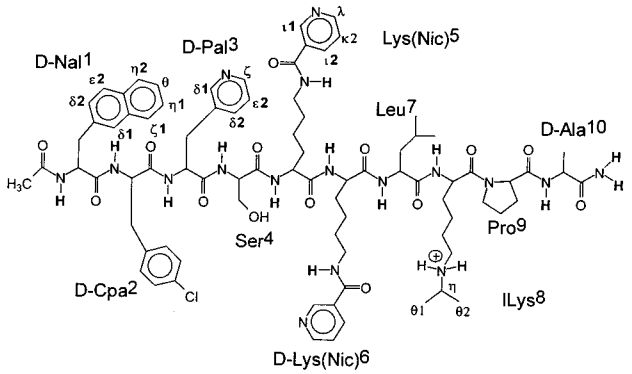

Figure 1. Schematic representation of antide. The nomenclature of hydrogen atoms and amino acids throughout the text follows the IUPAC−IUBMB−IUPAB recommendations (Markley, J. L.; et al. *Pure Appl. Chem.*, **1998**, *70*(1), 117−142). The nomenclature for the aromatic protons of residues D-Nal^1, D-Cpa^2, D-Pal^3, Lys(Nic)^5, D-Lys(Nic)^6, and the isopropyl group of Ilys^8 is shown.

(3) The exchange rate of the N^ϵ-amine protons of residue Ilys^8 observed at pH = 5.1, T = 280 K is slow enough to allow the observation of their ^{1}H NMR signals and to allow the transfer of magnetization between the protons of the isopropyl group and the ones of the lysine side chain in TOCSY experiments.

(4) The assignment of the nicotinoyl fragments of residues Lys(Nic)^5 and D-Lys(Nic)^6 has been done on the basis of the NOE peak observed between the $H^{\iota 2}$ proton of residue Lys-(Nic)^5 and the side-chain amide NH^ζ proton.

(5) The residue Pro^9 was found to be in the trans configuration, as clearly testified from the intense NOE signals between the H^α proton of residue Ilys^8 and both H^δ protons of Pro^9.

The results of resonance assignment are listed in Table 1. The pH titration of a D_2O solution of antide show no significant changes in the ^{1}H NMR signals of nonexchangeable protons within the pH* range 5.0−7.6, with the exception of a slight downfield shift (by about 0.05 ppm) of the Ilys^8 H^γ resonances (pH* refers to pH-meter readings uncorrected for isotope effect). As the pH approaches 7.6, a reduction of the intensity as well as a slight broadening of the NMR lines is observed, which is consistent with the known occurrence of aggregation phenomena and poor solubility shown by antide at physiological pH values. The lack of significant changes in the ^{1}H NMR chemical shifts suggests that no major changes of the conformation or protonation equilibria occurs within the pH* range 5.0−7.6. Below pH* = 5.0, the pyridine-like nitrogen of residue D-Pal^3 becomes charged and the resonances of the aromatic protons are consequently shifted downfield. The protonation at the nitrogen atoms of the nicotinoyl group of residue Lys(Nic)^5 and D-Lys-(Nic)^6 is found between pH* = 3.5 and 1.2, as detected by the marked downfield shift of the nicotinoyl resonances. The resonances of the Ilys^8 H^γ protons move from 0.4−0.47 ppm at a pH* value of 5.9 to 0.60−0.65 ppm at a pH* value of 1.2.

(B) Structure Calculations. A series of 2D-NOESY spectra were acquired at 280 K with mixing times of 120, 200, 300,

(26) Still, W. C.; Tempczyk, A.; Hawley, R. C.; Hendrickson, T. *J. Am. Chem. Soc.* **1990**, *112*, 6127−6129.
(27) Shenkin, P. S.; McDonald, D. Q. *J. Comput. Chem.* **1994**, *15*, 899−916.

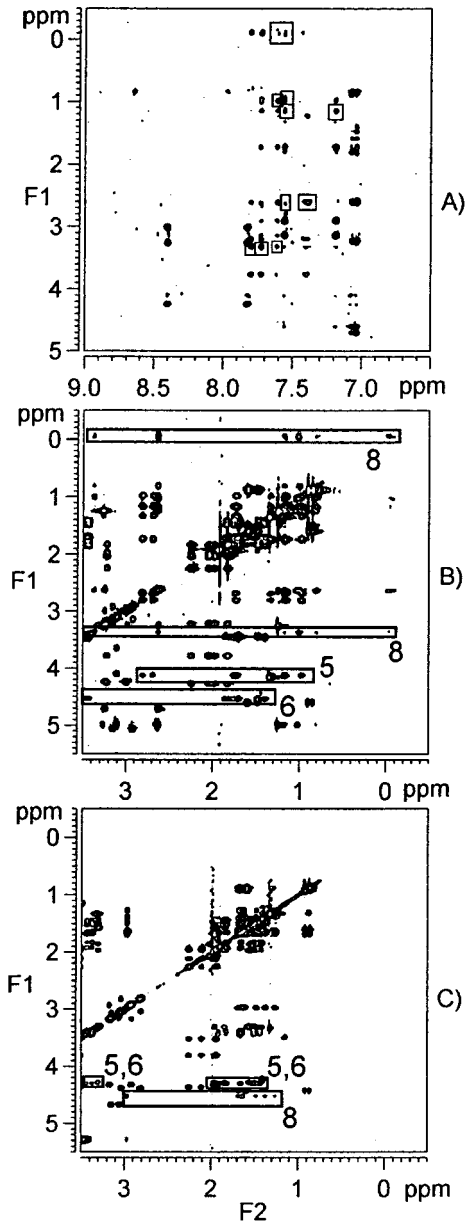

Figure 2. (A) Contour map of the F1 (−0.5/5.0 ppm), F2 (6.5/9.0 ppm) region of the NOESY spectrum of antide in D_2O solution (0.5 mM, pH* = 5.3, T = 280 K, mixing time 350 ms) showing the most relevant cross-peaks between the side chains of residues D-Nal[1] and Ilys[8] (squares). (B) Expanded region (F1, −0.5/5.5 ppm; F2, −0.5/3.5 ppm) of the 2D-TOCSY spectrum of antide in aqueous solution (0.5 mM, H_2O/D_2O 90%, pH = 5.1, T = 280 K) evidencing the difference in the ^{1}H NMR chemical shifts of the aliphatic side chain protons of the three lysine-like residues [Lys(Nic),[5] D-Lys(Nic)[6], and Ilys[8]]. The TOCSY strips parallel to the F2 axis, corresponding to the H^α diagonal peaks, are shown for each of these amino acids. For Ilys[8], the TOCSY strip corresponding to the H^γ diagonal peaks is also shown. (C) Expanded region (F1, −0.5/5.5 ppm; F2, −0.5/3.5 ppm) of the 2D-TOCSY spectrum of antide in TFE solution (3.5 mM, neat TFE-d_2-OH, T = 285 K). The TOCSY strips parallel to the F2 axis corresponding to the H^α diagonal peaks are shown for residues Lys(Nic)[5], D-Lys(Nic)[6], and Ilys[8]. Note that, in comparison with case B, the resonances of the aliphatic side chain protons of the three lysine-like residues are very close each other.

350, and 400 ms. The measured NOE peak intensities generally grew up to 300−350 ms and leveled off or decreased at longer mixing times. The NOESY spectra acquired with mixing times of 350 ms (both H_2O/D_2O 90% and D_2O solution) were used to derive the geometric constraints. No significant spin diffusion

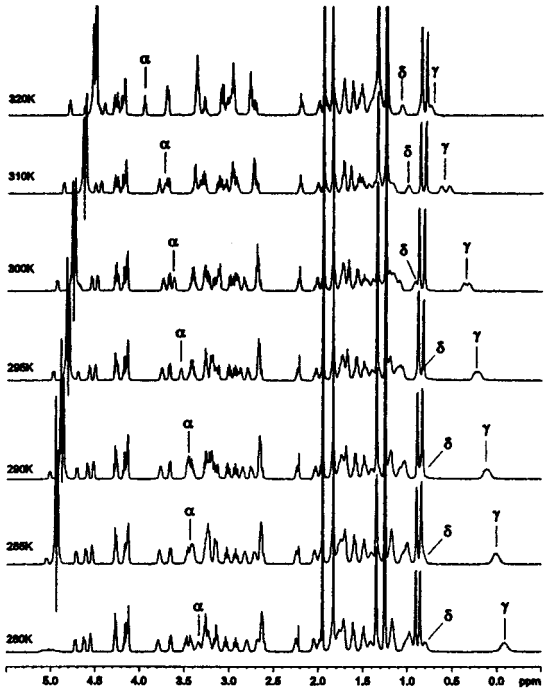

Figure 3. ^{1}H NMR spectra acquired at different temperatures of antide in D_2O solution (0.5 mM, D_2O, pH* = 5.7). The resonances of selected side-chain protons of Ilys[8] are marked.

effects were found at this mixing time. The analysis of such NOESY spectra allowed us to derive as many as 180 geometric constraints for TAD calculations (seven dihedral angle constraints from $^3J_{NH-H\alpha}$ were also included in the calculations). Among these distance constraints, 63 were intraresidue, 63 between sequential residues, and 54 were medium/long range (i.e., involving residues at least two positions far apart in the amino acid sequence; see Table 4). It is worth noting that 17 long-range NOE peaks were found between the aromatic protons of residue D-Nal[1] with the side-chain protons of residue Ilys[8] (best detected in D_2O solution, Figure 2A). In addition, a strong NOE contact was found between D-Nal[1] H^α and Leu[7] H^α, and five weak NOE contacts involved the side chain D-Nal[1] $H^{\epsilon 2}$/$H^{\eta 2}$ and Pro[9] H^δ protons. Both the high number of NOE contacts and the detection of unusual chemical shifts for residue Ilys[8] indicate a high degree of structuration of antide in aqueous solution. A more detailed picture of the conformation of antide can be obtained by a combination of molecular dynamics in the torsion angle space (TAD) with simulated annealing techniques and molecular mechanics techniques. Since no evidence was found about the presence of asymmetric dimers (all the NMR spectra showed invariably one resonance for each proton), the structural calculations were carried out following the hypothesis of a monomeric structure. Although in principle the peptide might also exist in the form of a symmetric dimer, this circumstance is unlikely, because of the irregular distribution of residues in D and L stereochemical configuration along the amino acid sequence.

One thousand random conformations were generated and independently energy minimized by constrained TAD and simulated annealing. An ensemble of 30 conformers endowed with the lowest residual target function values (e.g., showing the lowest constraints violations and the highest steric consistency) was then selected out of the bundle of 1000 optimized

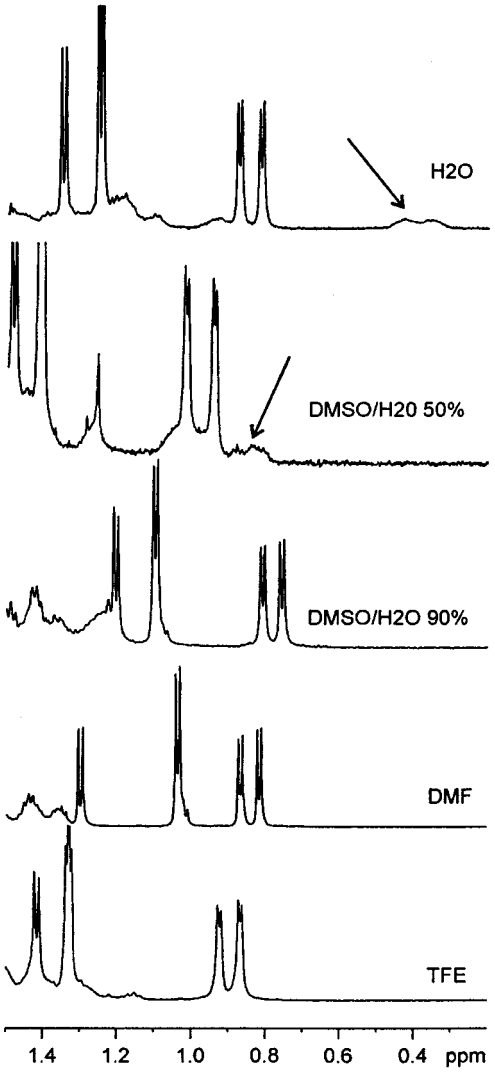

Figure 4. Aliphatic region (0.2−1.5 ppm) of the ^{1}H NMR spectra of antide in different solvents. The arrows indicate the ring current shifted signals from Ilys^8 H$^\gamma$ protons that can be considered as structural markers (see the text).

conformers and considered as representative of the structure of antide. The average target function value for these 30 structures was as low as 3.6×10^{-2} Å^2, indicating that the calculated structures fulfilled the NMR constraints and were sterically consistent. As a matter of fact, there was only one interproton distance showing a violation larger than 0.1 Å and none larger than 0.2 Å (Table 4). The 30 structures selected after restrained TAD were refined further by 10 ps constrained molecular dynamics at a temperature of 300 K followed by energy minimization. The refinement step was carried out with the AMBER force field, which allows for a more detailed treatment of the energetic terms due to nonbonded interactions. The refinement step afforded an ensemble of 30 structures having energies in the range −720 to −798 kJ/mol (mean −740 kJ/mol) and Lennard-Jones potential energies in the range 2.8 to −63.7 kJ/mol (mean −14.7 kJ/mol), confirming a satisfactory convergence of the energies and the good nonbonded geometry of the structures. A picture of a representative structure of antide is provided in Figure 6; a superposition of 10 optimized structures where the rmsd between the backbone atoms of residues 2−9 has been minimized is shown in Figure 5.

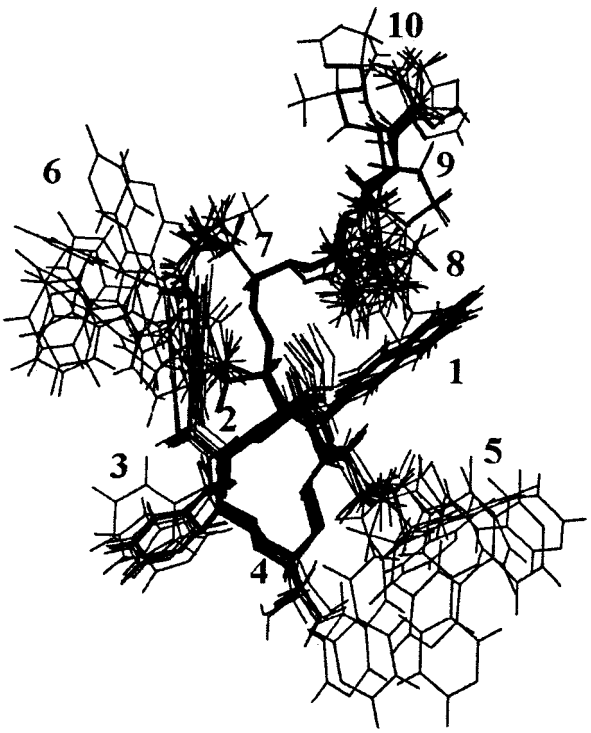

Figure 5. Superposition of 10 structures of antide (belonging to the δ2 family, aqueous solution) obtained by restrained TAD with simulated annealing and energy minimization. The rmsd between the backbone atoms of residues 2−9 has been minimized. The backbone bonds are plotted with thicker lines with respect to side-chains bonds. Note the spatial proximity of the side chains of residues D-Nal^1 and Ilys^8. This arrangement is responsible for the observed upfield shift of Ilys^8 side chain protons (mainly H$^\gamma$ and H$^\delta$) due to ring current shift effect.

In the final structures, the pairwise backbone rmsd calculated over the superposition of segment 2−9 has a value of 0.60 ± 0.29 Å, whereas the heavy atom rmsd for the same segment has a value of 2.22 ± 0.51 Å. This indicates a fairly good global definition of the backbone conformation, whereas the conformation of the side chain appears to be less clearly defined. To distinguish between local and global conformational convergence of the optimized structures, the backbone atomic rmsd values were calculated over three-residues segments (Table 6, third column). Segment 5−7 shows the best local convergence (rmsd 0.08 ± 0.05 Å), whereas the C-terminus is less defined (segments 7−9 and 8−10 having backbone rmsd values of 0.34 ± 0.27 and 0.49 ± 0.21 Å, respectively). The N-terminus segment encompassing residues 1−4 also shows a lower degree of local convergence than fragment 5−7, but this can be partly ascribed to the presence of two families of conformations (both consistent with the NMR constraints) differing for the local backbone conformation around residue Ser^4 (see below). The side chains of the residues belonging to segment 1−4 are relatively defined (heavy atom rmsd 0.76 ± 0.53 Å for segment 1−3, 0.78 ± 0.52 Å for segment 2−4). Among these side chains, the naphthyl moiety of the residue D-Nal^1 adopts a remarkably defined conformation, if it is considered that this residue is the N-terminus one. Not surprisingly, the side chains that are found to be more disordered are the ones of the lysine-like residues [mainly Lys(Nic)^5 and D-Lys(Nic)^6], being these residues endowed with a large number of torsional angles. As a matter of fact, the minimized heavy atom rmsd value relative to segment 5−7 is as high as 2.02 ± 0.54 Å. The residues

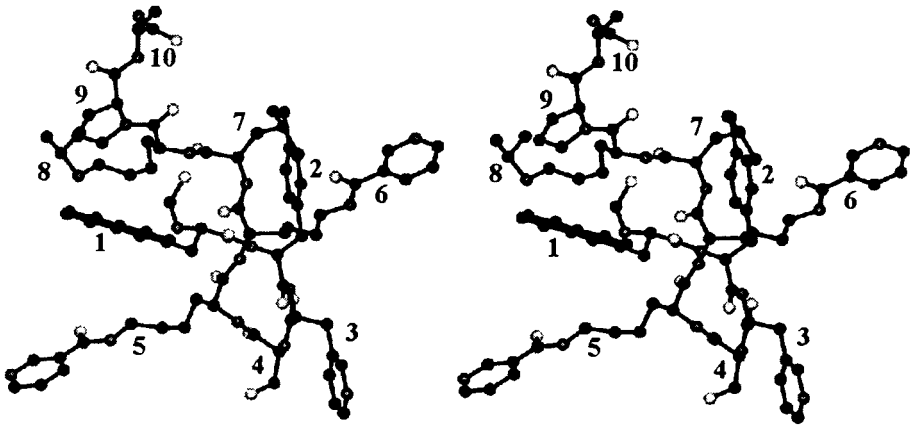

Figure 6. Stereoview of a representative structure of antide obtained in aqueous solution. This structure belongs to the family $\delta 1$ (see the text). Carbon, nitrogen, and oxygen atoms are given in black, dark gray, and light gray, respectively. The chlorine atom of residue D-Cpa[2] is black. No hydrogen atom is shown. The backbone dihedral angles of this structure are as follows: ϕ_1, 112°; ψ_1, −158°; ϕ_2, 79°; ψ_2, −162°; ϕ_3, 45°; ψ_3, −124°; ϕ_4, −118°; ψ_4, 10°; ϕ_5, −78°; ψ_5, −37°; ϕ_6, 108°; ψ_6, −147°; ϕ_7, −101°; ψ_7, 144°; ϕ_8, −95°; ψ_8, 129°; ϕ_9, −86°; ψ_9, 62°; ϕ_{10}, 69°; ψ_{10}, −83°. All peptide bonds are trans.

Table 5. Structure Calculation of Antide in Different Solvents. RMSD Values for the Backbone Atoms or Heavy Atoms of Selected Molecular Moieties after Structure Refinement by Means of MD and Energy Minimization (see the text)

	water				
	family $\delta 1$[a]	family $\delta 2$[b]	TFE[c]	DMF[c,d]	DMSO[c,d]
	Backbone rmsd (Å) ± sd				
residues 2−9	0.43 ± 0.22	0.59 ± 0.25	0.36 ± 0.17	1.55 ± 0.70	1.66 ± 0.54
residues 1−3	0.02 ± 0.01	0.12 ± 0.10	0.26 ± 0.14	0.52 ± 0.21	1.09 ± 0.38
residues 2−4	0.01 ± 0.01	0.09 ± 0.08	0.13 ± 0.06	0.34 ± 0.31	0.68 ± 0.26
residues 3−5	0.01 ± 0.01	0.06 ± 0.04	0.14 ± 0.06	0.29 ± 0.33	0.40 ± 0.27
residues 4−6	0.03 ± 0.02	0.08 ± 0.05	0.15 ± 0.09	0.29 ± 0.37	0.16 ± 0.13
residues 5−7	0.05 ± 0.03	0.07 ± 0.04	0.11 ± 0.07	0.51 ± 0.43	0.35 ± 0.30
residues 6−8	0.16 ± 0.10	0.09 ± 0.07	0.08 ± 0.04	0.66 ± 0.26	0.56 ± 0.24
residues 7−9	0.37 ± 0.25	0.17 ± 0.21	0.08 ± 0.05	0.73 ± 0.30	0.69 ± 0.32
residues 8−10	0.52 ± 0.19	0.43 ± 0.21	0.53 ± 0.24	0.68 ± 0.23	0.68 ± 0.22
	Heavy Atoms rmsd (Å) ± sd				
residues 2−9	1.96 ± 0.49	1.87 ± 0.41	1.98 ± 0.57	4.27 ± 1.01	4.52 ± 0.90
residues 1−3	0.10 ± 0.05	0.34 ± 0.25	0.75 ± 0.34	1.96 ± 0.63	2.86 ± 0.65
residues 2−4	0.24 ± 0.15	0.28 ± 0.19	0.71 ± 0.45	1.49 ± 0.82	1.92 ± 0.60
residues 3−5	1.63 ± 0.66	1.65 ± 0.52	1.29 ± 0.61	2.61 ± 0.90	2.62 ± 0.76
residues 4−6	1.97 ± 0.62	1.89 ± 0.46	1.80 ± 0.64	3.23 ± 0.97	2.85 ± 0.75
residues 5−7	2.00 ± 0.61	1.88 ± 0.47	1.80 ± 0.65	3.30 ± 0.88	3.06 ± 0.75
residues 6−8	1.65 ± 0.44	1.38 ± 0.31	1.89 ± 0.56	3.13 ± 0.77	3.00 ± 0.67
residues 7−9	1.32 ± 0.37	1.10 ± 0.27	1.15 ± 0.51	1.96 ± 0.45	2.11 ± 0.53
residues 8−10	1.66 ± 0.42	1.38 ± 0.37	1.48 ± 0.52	2.01 ± 0.52	1.92 ± 0.47

[a] rmsd values calculated over an ensemble of 13 conformers out of 30 total. [b] rmsd values calculated over an ensemble of 17 conformers out of 30 total. [c] rmsd values calculated over an ensemble of 30 conformers. [d] The structures obtained by DYANA calculations were not refined.

Table 6. Comparison of the Structures of Antide in Aqueous and TFE Solutions. Pairwise Backbone rmsd Values after Local Backbone Superposition of the S-Conformation (TFE) with the $\delta 1$- and $\delta 2$-Conformations (water)

backbone segment	pairwise backbone rmsd after local backbone superposition of conformations (Å) ± sd		
	S and $\delta 1$	S and $\delta 2$	$\delta 1$ and $\delta 2$
residues 2−9	1.04 ± 0.81	0.97 ± 0.67	0.60 ± 0.29
residues 1−3	0.41 ± 0.25	0.51 ± 0.32	0.26 ± 0.19
residues 2−4	0.48 ± 0.44	0.45 ± 0.36	0.27 ± 0.21
residues 3−5	0.41 ± 0.35	0.41 ± 0.31	0.31 ± 0.26
residues 4−6	0.37 ± 0.30	0.21 ± 0.12	0.34 ± 0.27
residues 5−7	0.26 ± 0.19	0.26 ± 0.18	0.08 ± 0.05
residues 6−8	0.40 ± 0.38	0.41 ± 0.36	0.16 ± 0.13
residues 7−9	0.37 ± 0.34	0.46 ± 0.40	0.34 ± 0.27
residues 8−10	0.57 ± 0.23	0.59 ± 0.23	0.49 ± 0.21

belonging to the C-terminus part of the molecule show intermediate heavy atom rmsd values (1.54 ± 0.41 Å for segment 6−8 and 1.34 ± 0.38 Å for segment 7−9).

Despite the lack of regular secondary structure motifs, the conformational analysis reveals that the backbone of antide adopts a defined, δ-shaped conformation in aqueous solution (for the sake of simplicity, we will refer to the water conformation as the δ-conformation in the text; see Figure 8). The global folding of the antide backbone presents a turn centered at residues D-Pal[3]-Ser[4], followed by a segment (residues 5−10) endowed with a more extended conformation. The ϕ and ψ dihedral angle values at the residues involved in the turn (D-Pal[3]-Ser[4]) as well as the hydrogen bonding and NOE patterns are not consistent with a regular β-type or γ-type turn. The only consistent hydrogen bond (found in all the optimized structures) involves D-Cpa[2] NH and D-Lys(Nic)[6] CO. Nine out of 30 structures also present a hydrogen bond between D-Ala[10] NH and Ilys[8] CO. The overall folding scheme of antide brings the side chains of residues D-Nal[1] and Ilys[8] very close each other. As a matter of fact, the most striking feature common to all the optimized structures is the close proximity of the naphthyl ring of D-Nal[1] to the aliphatic side chain of Ilys,[8] which lays just below the plane of the naphthyl moiety (see Figures 5, 6, and 9). Such a spatial arrangement provides a rationale for the observed upfield shift of the side chain Ilys[8] protons, which can be safely attributed on the basis of this conformational model to a ring current shift effect induced by the naphthyl moiety. The high upfield shift of Ilys[8] H^{γ} protons together with the high number of NOE observed between these protons and the naphthyl ones moreover indicates the remarkable stability of this spatial arrangement. Such a stability probably arises both from hydrophobic interactions and steric hindrance effects, being the naphthyl ring sandwiched between the bulky side chains of residues Ilys[8] and Lys(Nic).[5] Residue Lys(Nic)[5] also shows somewhat upfield-shifted side chain proton resonances, being consistent with ring current shift effects. It is worth observing that the δ-conformation showing the D-Nal[1]/Ilys[8] interaction motif was obtained also when the molecular dynamics calculations were repeated, excluding the long-range NOE distance constraints connecting the side chain of these residues.

A closer inspection of the bundle of the 30 energy-minimized structures reveals that two families of conformers are actually present. These families can be clearly identified by cluster analysis. The optimized structures were superposed along the

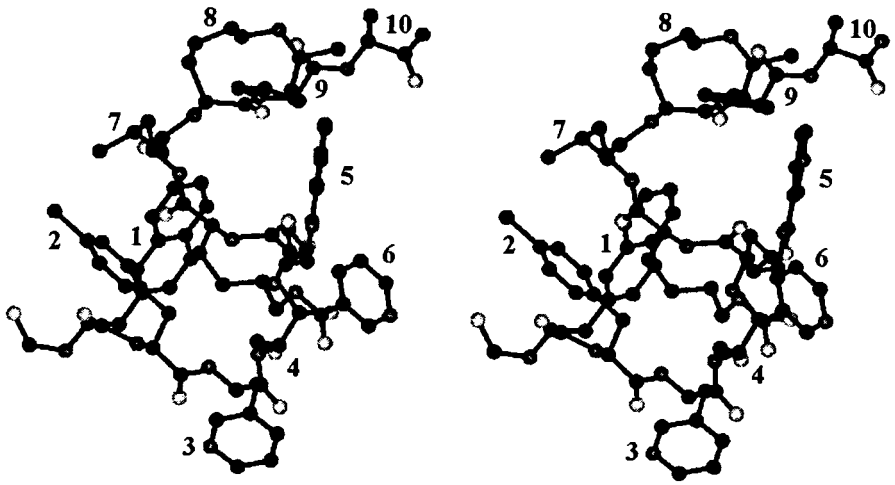

Figure 7. Stereoview of a representative structure of antide obtained in TFE solution. Carbon, nitrogen, and oxygen atoms are given in black, dark gray, and light gray, respectively. The chlorine atom of residue D-Cpa[2] is black. No hydrogen atom is shown. The backbone dihedral angles of this structure are as follows: ϕ_1, 168°; ψ_1, 108°; ϕ_2, 158°; ψ_2, −169°; ϕ_3, 46°; ψ_3, 46°; ϕ_4, −167°; ψ_4, −43°; ϕ_5, −144°, ψ_5, −70°; ϕ_6, 140°; ψ_6, −157°; ϕ_7, −68°; ψ_7, −33°; ϕ_8, −166°; ψ_8, 169°; ϕ_9, −87°; ψ_9, 176°; ϕ_{10}, 171°, ψ_{10}, −161°. All peptide bonds are trans.

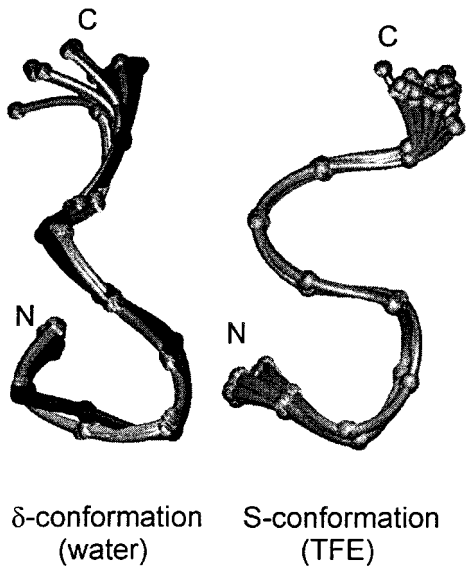

Figure 8. Ribbon representations of the structure of antide showing the δ-conformation (water) and the S-conformation (TFE). δ-conformation: backbone superposition (fitted to residues 2−9) of 20 energy-minimized conformers. The black structures are from family $\delta 1$ (10 structures) and the gray ones from family $\delta 2$ (10 structures). S-conformation: backbone superposition (fitted to residues 2−9) of 20 energy-minimized conformers. See Table 5 for pairwise backbone rmsd values.

backbone heavy atoms of residues 2−9, and the atomic root-mean-square displacement between pairs of structures was calculated. Such rms displacements can be considered as a measurement of the conformational distance between a given pair of structures. The rms displacements were then analyzed in order to assess whether the ensemble of conformations could be split into structurally related groupings (clusters) or whether the conformations were distributed in a continuous manner. The conformers clearly group into two families of structures: family $\delta 1$ (13/30 members, backbone rmsd value over segment 2−9 of 0.43 ± 0.22 Å) and family $\delta 2$ (17/30 members, backbone RMSD value over segment 2−9 of 0.59 ± 0.25 Å). To better identify the structural determinants that are responsible for the grouping into two classes of structures, the cluster analysis was repeated by using the rms displacements calculated after

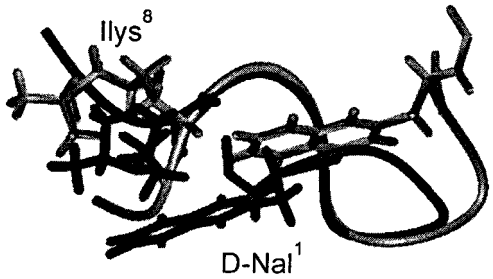

Figure 9. Backbone superposition (ribbon representation) over segment 4−8 of the lowest energy structures of antide obtained for aqueous solution (black) and TFE solution (gray). The side chains of residues D-Nal[1] and Ilys[8] are also shown. Note the proximity of the naphthyl ring belonging to residues D-Nal[1] and the side chain of Ilys[8] in the structure obtained from aqueous solution.

superposition of shorter backbone segments. It was found that the grouping into families $\delta 1$ and $\delta 2$ is strictly dependent on the local backbone conformation around residue Ser[4]. Family $\delta 1$ shows a better convergence of the backbone conformation in the segment 1−5 than family $\delta 2$, as can be argued by comparing the pairwise backbone rmsd values calculated separately for each family (listed in Table 5).

Variable-temperature measurements allow us to estimate the relative stability of the structural motifs. The ring current shifted signals of residue Ilys[8] [and to a less evident extent the ones of Lys(Nic)[5]] move downfield linearly as the temperature increases. As marked by the chemical shift of Ilys[8] H^{γ} and H^{δ} protons, the δ-shaped conformation is still maintained at a temperature as high as 320 K. These findings support the view of a progressive temperature-dependent loosening of the δ-conformation rather than the occurrence of an abrupt conformational change. Further insights into the mobility of backbone segments can be obtained by the analysis of (i) the chemical shift temperature coefficients $\Delta\delta/\Delta T$ of backbone amide protons and (ii) the solvent-accessible surface calculated from the optimized molecular models. The $\Delta\delta/\Delta T$ coefficients of backbone amide protons are positive (chemical shifts increase as the temperature increases) for the backbone amide protons of Ilys[8] and D-Lys(Nic)[6], whereas the other amide protons have negative $\Delta\delta/\Delta T$ values (chemical shifts decrease as the temperature increases), falling in the range −2.1 to −15.2 ppb/K (Table 3). The small

or positive $\Delta\delta/\Delta T$ values of Lys(Nic),[5] D-Lys(Nic)[6], and Ilys[8] backbone NH indicate that such protons are not accessible to the solvent. Consistently, solvent accessible surface calculations for such amide protons in the optimized models yielded very small or null values, supporting the view that these protons are deeply buried within the antide molecule (Table 3) and cannot be reached by water molecules. On the other hand, the backbone amide protons of D-Nal[1], Leu[7], and D-Ala[10] are characterized by both large $\Delta\delta/\Delta T$ values and high calculated solvent accessible surfaces, indicating that these protons are freely accessible to water molecules. Finally, the amide protons belonging to residues D-Cpa[2], D-Pal[3], and Ser[4] show considerably high $\Delta\delta/\Delta T$ coefficients, but the relative calculated solvent accessible surface is minimal or null. The discrepancy between $\Delta\delta/\Delta T$ values and calculated solvent accessible surface is even more evident in the case of the D-Cpa[2] NH proton, which is found to be hydrogen bound to the backbone D-Lys(Nic)[6] CO group in all the minimized structures. Such a discrepancy may be explained by taking into account that increasing temperatures may lead to local structural rearrangements such that the amide protons become more exposed to the solvent. Thus, the molecular segment encompassing residues 2−4 must be endowed with some degree of conformational mobility. The energy-minimized molecular models (families $\delta 1$ and $\delta 2$, obtained from NMR data acquired at 280 K) from which accessibility data were calculated must then be regarded as limiting conformations. Other conformational possibilities where a significantly higher solvent accessible surface is allowed for D-Cpa[2], D-Pal[3], and Ser[4] amide protons may be envisaged to become more populated at higher temperatures.

Organic Solvents. As a general feature of ^{1}H NMR spectra of antide in organic solvent solution (DMSO/H_2O 90%, DMF, TFE), it is observed that the signals due to Ilys[8] H^γ protons (found to be upfield shifted to 0.40 ppm in aqueous solution at 300 K) are endowed with more typical chemical shift values (in the range 1.2−1.8 ppm). Since such signals are characteristic of the aqueous δ-conformation, it may be forwarded that antide adopts a different conformation in DMSO, DMF, and TFE with respect to the aqueous solution. However, it is worth noting that, as far as evaluated by the chemical shifts of the Ilys[8] H^γ protons, the δ-conformation of antide is at least partially retained in water/DMSO mixtures containing up to 50% v/v DMSO (Figure 4). Resonance assignment of ^{1}H NMR spectra carried out in DMSO/H_2O 90%, DMF, and TFE shows that the spread in the chemical shifts of the side-chain protons of the three lysine-like residues is greatly reduced with respect to water, suggesting that these side chains sample on average a similar chemical environment.

Structure Calculations. (A) Trifluoroethanol. Although no evidence about the occurrence of the δ-shaped conformation could be found on the basis of the chemical shift of Ilys[8] side-chain protons, 2D-NOESY experiments afforded a large number of meaningful constraints for MD calculations (Table 4). The NOESY spectrum obtained with a mixing time of 300 ms (at 285 K) was chosen to derive NOE peak volumes, because under these conditions the maximum intensity of NOE peaks is obtained while spin diffusion artifacts are negligible. Among a total number of 193 upper distance bounds, 112 were intraresidue, 58 were sequential, and 23 were medium/long-range. The detection of NOE peaks between Ilys[8] H^α-Pro[9] H^δ and between Ilys[8] HN-Pro[9] H^δ indicates that the trans geometry at the Ilys[8]-Pro[9] peptide bond is maintained in TFE solution. Remarkably, only one weak NOE contact was found between the D-Nal[1] naphthyl ring protons and residue Ilys.[8] All the 193 upper distance bounds were used in TAD structure optimization calculations, which were carried out by following the same methodology used to obtain the structure of antide in aqueous solution. After minimization of an initial set of 1000 random conformers by means of TAD, 30 structures showing the best consistency with the NMR restraints were selected for further structure optimization. The average target function value of the selected structures was 1.1×10^{-1} Å^2 and no consistent violation of van der Waals distances was found. Only three out of 193 upper limit bounds were violated by more than 0.1 Å and there was no violation larger than 0.2 Å (see Table 4). To check the convergence of the molecular energies, the structures were refined further by 10 ps constrained MD simulations followed by energy minimization within the AMBER force field. After the refinement step, the energies ranged from −495 to −627 kJ/mol (mean −569 kJ/mol), whereas Lennard-Jones potential energies ranged from −2 to −46 kJ/mol (mean −23 kJ/mol). The rmsd between the backbone atoms of residues 2−9 of the final 30 structures is 0.36 ± 0.17 Å, whereas the heavy atom rmsd value is 1.98 ± 0.57 Å. The overall definition of the optimized structures is comparable to the one found in the case of aqueous solution, as can be argued by comparing the global and local rmsd values listed in Table 5. A stereoview of a representative structure obtained in TFE solution is given in Figure 7. The peptide backbone shows two irregular turns centered at residues Ser[4] and Leu[7] such as to yield a S-shaped conformation (S-conformation, depicted in Figure 8). The first turn involves the same region as found in aqueous solution, but with a different conformation. The dihedral angle values for the residues involved in the turns do not fall into a well-defined type of turn, as also indicated by the lack of expected hydrogen bonds. The family of calculated structures does not show a well-defined hydrogen-bonding pattern [the most conserved hydrogen bonds are (i) between D-Ala[10] NH and Ilys[8] CO found in nine out of 30 energy-minimized structures and (ii) between the C-terminus amido group and Pro[9] CO, found in five out of 30 structures]. As expected from the lack of significant long-range NOE contacts and from the lack of ring current shifted signals, the side chains of residues D-Nal[1] and Ilys[8] are not facing each other within the S-shaped conformation (Figure 9). On the basis of the rmsd calculated by the superposition of backbone segments between the TFE structural model and the $\delta 1$ and $\delta 2$ ones, it is found that the backbone region that appears to be less affected by environmental changes (water and TFE) is the one encompassing residues 5−7 (see Table 6).

(B) DMF. Despite the analysis of NOESY spectra (mixing time 350 ms, $T = 280$ K) affording as many as 141 upper limit bounds, TAD with simulated annealing calculations did not converge to a well-defined family of conformations in the case of DMF solution. The backbone rmsd and heavy atom rmsd minimized within segment 2−9 have values of 1.55 ± 0.70 and 4.27 ± 1.01 Å, which are quite high values for a peptide of this size. These structures were not further refined. Although the structures are not clearly defined, the backbone conformation of antide in DMF presents two ill-defined turns centered at

segments 3−4 and 5−8. On a relative scale, the backbone segment that appears to be locally more defined is the one encompassing residues 3−6.

(C) DMSO/Water 90%. 2D-NOESY spectra (mixing time 300 ms, $T = 290$ K) afforded a limited number of upper limit distances (Table 4), especially if medium/long-range upper limit distances are considered. Structure calculations by TAD consequently did not converge to any well-defined family of structures as shown by the high backbone and heavy atom rmsd values (1.66 ± 0.53 and 4.52 ± 0.90 Å, respectively, minimized with respect to residues 2−9; see also Table 5). The structures obtained by means of TAD with simulated annealing were not further refined. These data clearly indicate that, when DMSO is present at high percentages in the solvent mixture, antide becomes endowed with a largely random coil structure. On the basis of the comparison of the local backbone rmsd values, the region that appears to be best defined within the ensemble of conformation obtained in DMSO is the one encompassing residues 4−6.

Discussion

The preferential conformation adopted by antide in water solution brings about the two ends of the molecule in such a way that the side chains of residues D-Nal[1] and Ilys[8] are very close in space. This motif produce a remarkable upfield shift of the side-chain protons of Ilys[8] (especially the H^{γ} ones), which is strictly characteristic of the water δ-conformation (this effect was not observed in the organic solvent solutions considered so far). Since ring current shift effects are very sensitive to internuclear distances and molecular motions, the chemical shifts of Ilys[8] H^{γ} protons then behave as very sensitive structural markers. Thus, the simple observation of the Ilys[8] H^{γ} chemical shifts may be used to assess at least in qualitative terms the presence of the δ-shaped conformation of antide under different conditions (temperature, pH, solvent). The increased conformational mobility of the molecule induced by high temperatures is paralleled by the downfield shift of Ilys[8] H^{γ} resonances, which still experience a substantial ring current shift contribution at a temperature as high as 320 K**.** Thus, increasing temperatures produces a loosening of the antide conformation rather than a severe disruption of the peptide fold to yield a fully mobile, random coil conformation. The measured $\Delta\delta/\Delta T$ coefficients and calculated solvent accessibility surfaces of the backbone amide protons point out that the backbone segment 2−4 is locally more subjected to the temperature-induced increase of conformational freedom than the remaining backbone moiety is. As far as guessed by Ilys[8] H^{γ} resonances, also pH changes within the range 1.2−7.6 do not produce major conformational changes. Thus, the structure of antide in aqueous solution is stable, even though the molecule acquires four positive charges [protonation of the aromatic side chains of residues D-Pal[3], Lys(Nic)[5], and D-Lys(Nic)[6], in addition to the Ilys[8] amino group]. The structure marker signals indicate the presence of the δ-shaped conformation in DMSO/H_2O 50% v/v mixture (Ilys[8] H^{γ} signals at about 0.83 ppm, broad), whereas they indicate the loss of the δ-shaped conformation when the molecule is dissolved in organic solvents or mixtures containing high organic solvent percentages. All these data support the view of a remarkable stability of the antide δ-shaped water conformation and suggest that the same conformation may be the biologically relevant one. The conformational state of antide in membrane mimicking environments (micelles) is currently under investigation in order to confirm this hypothesis.

The high degree of structuration of such a small peptide raises the question regarding the origin of the molecular forces that are responsible for the folding. Such forces may have an intramolecular origin (i.e., electrostatic interactions, steric repulsions) as well as an intermolecular origin (water may drive the folding by hydrophobic effects). To tackle this problem, we resorted to the analysis of the contribution of water solvation to the total energy of the molecular models obtained in aqueous solution (δ-conformation) and TFE solution (S-conformation). The MD calculations that led to the δ- and S-conformations have been carried out in vacuo, and the structures obtained from these calculations are heavily biased by the NOE-derived experimental constraints. In the ensuing discussion, we make use of the approximation that the δ- and S-conformations faithfully describe the structure adopted by antide in aqueous solution and TFE solution respectively, even though no solvent treatment was included in the structure optimization calculations. This approximation is justified by the fact that the NOE constraints have a larger weight toward the determination of the conformational preferences of antide than solvation effects have. The experimental δ- and S-conformations were then subjected to energy minimization within the AMBER force field, including water solvation effects. The treatment of the solvent was done according to the generalized Born/surface area (GB/SA) continuum solvation model,[26] which affords solvation free energies (i.e., free energies differences associated with moving the molecule from vacuum to the water phase). When the energies of the two models were calculated both accounting for water solvation, the δ-conformation had a solvation free energy contribution of −497.0 kJ/mol and a total energy of −1265.9 kJ/mol, whereas the S-conformation a had a solvation free energy contribution of −559.7 kJ/mol and a total energy of −1165.1 kJ/mol. Although the S-conformation is the one experimentally found in TFE solution, it is slightly better solvated by water than the δ-conformation (experimentally obtained from aqueous solution). This fact points out that water solvation effects toward the stabilization of the δ-conformation with respect to the S-conformation must be small. On the other hand, the intramolecular energies as far as evaluated by MM in vacuo of the δ-conformation and S-conformation are −834.0 and −745.4 kJ/mol, respectively. This indicates that the δ-conformation is energetically more favorable than the S-conformation. These data convey the view that the δ-conformation of antide is driven by intramolecular forces rather than by water-solvation effects. Then, the conformational change observed on going from water to TFE must be due to the ability of the latter solvent to disrupt the intramolecular interactions. The same arguments may be applied to DMF and DMSO, with the noticeable exception that such solvents do not induce a defined conformation as TFE does.

Conclusions

Antide adopts in water solution a defined δ-shaped conformation, which is basically characterized by an irregular turn at residues D-Pal[3]-Ser[4] and by the close spatial proximity of the

side chains belonging to D-Nal[1] and Ilys[8]. This conformation is remarkably stable around the side-chain D-Nal[1]-Ilys[8] interaction motif and about the backbone segment 5−7. The stability of the δ-shaped conformation makes it possible to infer that no major changes are likely to occur upon receptor binding, although some possibilities for different biologically active backbone local conformations are left for the segment 2−4 and around the C-terminal D-Ala[10] segment. The δ-shaped conformation of antide shows the conformational requirements that are known[6,14a] to play a key role toward the receptor binding affinity, i.e., (i) the presence of a turn in the backbone and (ii) the all-trans nature of the peptide bonds. The structural rigidity of antide likely adds a further contribution to the binding affinity, because of the lower entropic term in the complex formation. The backbone turn of antide is irregular and it is located at residues 2−5 rather than in the segment 4−8, as found in the case of dicyclic analogues of GnRH.[13,14] This finding enforces the view that the exact location of the turn along the backbone is not a key feature with respect to the receptor binding affinity, provided that the chain reversal brings the side chains of the crucial amino acids in the proper spatial orientation.[6,15] In this view, the D-Nal[1]/Ilys[8] side chain motif may be a relevant determinant for the molecular recognition process. The importance of nonbonded interactions and steric hindrance toward the stabilization of the biologically active conformation may offer a new criterion for the design of drugs conformationally constrained by noncovalent interactions.

List of Abbreviations

NMR, nuclear magnetic resonance; 2D-TOCSY, total correlation spectroscopy; NOE, nuclear Overhauser effect; 2D-NOESY, nuclear Overhauser effect spectroscopy; 2D-DQF−COSY, double quantum filtered correlation spectroscopy; PFG: pulse field gradient; TPPI, time proportional phase increment; rmsd, root mean square deviation; TAD, torsion angle dynamics; MD, molecular dynamics; MM, molecular mechanics; D-Nal, β-[2-naphthyl]-D-alanine; D-Cpa, D-*p*-chlorophenylalanine; D-Pal, β-[3-pyridyl]-D-alanine; Lys(Nic), $N\epsilon$-nicotinoyllysine; Ilys: $N\epsilon$-isopropyllysine; antide, *N*-Ac-D-Nal[1]-D-Cpa[2]-D-Pal[3]-Ser[4]-Lys(Nic)[5]-D-Lys(Nic)[6]-Leu[7]-Ilys[8]-Pro[9]-D-Ala[10]-NH_2; GnRH, gonadotropin releasing hormone (or LHRH, luteinizing hormone releasing hormone); TFE, 2,2,2-trifluoroethanol; DMSO, dimethyl sulfoxide; DMF, *N*,*N*-dimethylformamide; TMS, tetramethylsilane.

Acknowledgment. Authors gratefully acknowledge Prof. C. Luchinat and Prof. I. Bertini (CERM, University of Florence, Italy) for helpful discussion.

Supporting Information Available: Listing of all the upper limit distances used to obtain the structural models of antide in aqueous solution (Table S1) and TFE solution (Table S2). This material is available free of charge via the Internet at http://pubs.acs.org.

JA0115464